The investigation of an unstable convective flow using optical methods

M. Miozzi, G. Querzoli, and G. P. Romano
Dept. Mechanics and Aeronautics, University ''La Sapienza'' Via Eudossiana 18 00184 Roma, Italy

The convective flow field in a vessel is investigated by laser Doppler Anemometry (LDA) and Particle Image Velocimetry (PIV, namely Particle Tracking Velocimetry—PTV). The vessel is heated from below along a linear element at a temperature higher than that of the fluid. Hot fluid raises up and generates two counterrotating vortices. For a given aspect ratio, the two vortices become unstable and start to oscillate on a vertical plane (orthogonal to the heating element). This regime is investigated for increasing Rayleigh numbers to analyze the transition from regular to irregular conditions. The main transition mechanism is observed to be mostly connected to type II intermittency, a mechanism not frequently observed in experiments. However, at some Rayleigh numbers the present data does not definitely rule out type III intermittency. The phenomenon is analyzed by looking at the main frequencies in the spectrum of the horizontal velocity component and their changes with the Rayleigh number at a point above the heating element. Modifications in the local energy spectrum are analyzed by using the Wavelet Transform (WT) tool. Data obtained by PTV measurements make it possible to point out the spatial configuration of the flow and to determine the two velocity components on the measurement plane. These data are used to clarify the fundamental mechanisms of the transition. Instabilities are observed as sudden changes between two regimes of oscillations of the two counterrotating vortices: the first is characterized by oscillations centered on the vertical axis and the second by nonsymmetrical oscillations. © *1998 American Institute of Physics.* [S1070-6631(98)02308-3]

I. INTRODUCTION

Convective flows in closed vessels are mostly driven by external temperature differences: three main geometrical configurations are classically described:

(i) the one-dimensional Welander[1] configuration, where a pipe loop (radius much smaller than the overall length) is simultaneously heated from the bottom and cooled from the top;

(ii) the two-dimensional Rayleigh–Benàrd configuration (the amount of literature on the subject is enormous; see Koschmieder[2] for a review), in which a box with height much smaller than its width is considered and the bottom and top side are at different but uniform temperature (usually higher at the bottom);

(iii) the three-dimensional configuration, where only some portion of the bottom of the box (and sometimes a lateral side) is heated.

The linear heating element models fall within the last class. Ideally, the element is a line, but, whenever the length of the element is large in comparison with its width, the three-dimensional flow is reduced to two dimensions (at least for small temperature differences). This problem is particularly interesting for several industrial applications and fundamental research: cooling of devices in micro-electronic component design, environmental studies on pollutant, heat diffusion from quasi-linear sources, investigation of instabilities in fundamental thermo-fluid dynamic.

In a convective flow, as the value of the control parameters increases, transitions from one flow regime to another take place through sudden changes in the behavior of some measured quantity (for example, the temperature or one velocity component in a point of the flow field). However, in comparison to other flow fields, the transition regions are separated by large intervals where the measured quantities show almost the same behavior (Krishnamurti[3,4]).

The Rayleigh number is usually chosen as the main control parameter. It may be written as the ratio between the product of thermal and viscous diffusion timescales and the square of the time scale for buoyancy effects (Lesieur[5]):

$$\mathrm{Ra} = \tau_t \tau_v / \tau_g^2, \tag{1}$$

where $\tau_t = H^2/k$ and $\tau_v = H^2/\nu$ are the thermal and viscous diffusion time scales (H is the characteristic distance between hot and cold surfaces in the box, k is the thermal diffusivity of the fluid, and ν its kinematic viscosity). The time $\tau_g = 1/N_{\mathrm{BV}} = (H/g\alpha\Delta T)^{1/2}$ is the timescale for buoyancy effects (N_{BV} is the Brunt–Vaisäla frequency, g is the gravity acceleration, α is the thermal expansion coefficient, and ΔT is the temperature difference). The Rayleigh number depends on the temperature difference, but it gives no information on the predominant timescale for diffusive phenomena. To this end, the Prandtl number is usually employed (written as the ratio between the time scales for thermal and viscous diffusion),

$$\mathrm{Pr} = \tau_t / \tau_v. \tag{2}$$

These timescales allow to describe the behavior of a convective flow for increasing values of the control parameters Ra and Pr. For $\mathrm{Ra} < \mathrm{Ra}_c \approx 2000$ (where Ra_c is a critical Rayleigh number), at whatever Prandtl number, the flow
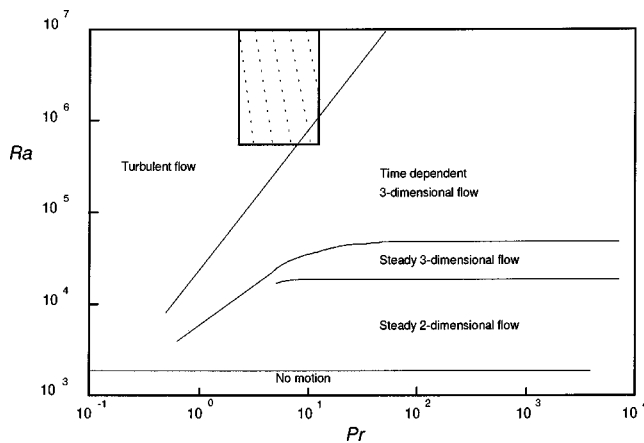
     2995

FIG. 1. The regime diagram (after Krishnamurti in Refs. 3,4). The different flow regimes are separated by continuous lines. The rectangular region bounds the present experimental conditions: in this region dotted lines show the way for Rayleigh and Prandtl numbers to be changed for each water-glycerol mixture.

field is at rest: τ_t is too small, in comparison with τ_g, to induce a global motion. For larger Rayleigh numbers (and Pr>1), temperature gradients are still smoothed very rapidly and buoyancy effects are meaningful for large time intervals only: the flow is steady. On the other hand, for even higher Rayleigh number, hot and cool regions are definitely separated: their location in respect to external heating and cooling elements and their motion under the influence of disturbances have to be considered. The flow field is time dependent and usually oscillatory. A further increasing in Rayleigh number leads to the turbulent regime. At a given Rayleigh number, instabilities appear only at low Prandtl numbers: this fact reflects the phenomenon that for low Prandtl numbers, instabilities are basically driven by viscous diffusion and by the ratio (τ_v/τ_g) (Newell and Whitehead[6]). In these conditions, from Eqs. (1) and (2), $(\tau_v/\tau_g) \sim (\text{Ra}/\text{Pr})^{1/2}$ which decreases as the Prandtl number increases. Viceversa, for high Prandtl numbers, instabilities are driven by thermal diffusion and by the ratio (τ_t/τ_g): from (1) and (2) it is $(\tau_t/\tau_g) \sim (\text{Ra Pr})^{1/2}$ which increases as the Prandtl number increases. These behaviors are summarized on a Pr-Ra diagram (Fig. 1 after Krishnamurti[3,4]): this diagram is properly derived for Rayleigh–Bénard convection, nevertheless it shows common features of many convective flows.

In the past the attention was mainly focused on steady two- and three-dimensional flow regions and on the transition to the time-dependent three-dimensional flow region (Krishnamurti,[3,4] Busse and Whitehead,[7] Bolton et al.,[8] Clever and Busse[9]). In these regions the flow is not turbulent.

In this paper the linear heating element configuration is considered: a rectangular vessel is heated from below along a linear channel. The main flow configuration consists of two vertical counterrotating vortices (convective rolls): such vortices appear on a plane orthogonal to the linear element and fill the whole vessel. When the temperature difference is increased ($\text{Ra}>10^6$) the two vortices exhibit regular oscillations on the vertical plane as observed numerically (Desrayaud and Lauriat[10]) and experimentally (Moses et al.[11]).

Noninvasive optical techniques (Laser Doppler Anemometry, LDA and Particle Tracking Velocimetry, PTV) are used to clarify the physical mechanisms leading to instabilities and in particular to analyze the transition to the turbulent regime (rectangular region in Fig. 1). Spectral and Wavelet Transform analysis are applied to LDA and PTV data to clarify the dynamics of the system for increasing Rayleigh numbers.

In Sec. II some physical consideration on the propagation of thermal disturbances are reported. The experimental setup for LDA and PTV measurements are described in Sec. III. Results are presented in Sec. IV and concluding remarks are given in Sec. V.

II. THE PROPAGATION OF THERMAL DISTURBANCES

Newell and Whitehead[6] give a timescale for the propagation of a thermal disturbance in a fluid over a distance H:

$$\tau_d = [(\text{Pr}+1)/\text{Pr}]\tau_t. \tag{3}$$

For $\text{Pr}\ll 1$ $\tau_d \approx \tau_v$, while for $\text{Pr}\gg 1$ $\tau_d \approx \tau_t$ as already mentioned. Another useful timescale is that for a fluid particle to cover one revolution along a roll (Schlüter et al.[12]):

$$\tau_0 = [\text{Ra}_c/(\text{Ra}-\text{Ra}_c)]^{1/2}\tau_t, \tag{4}$$

where Ra_c is the critical Rayleigh number for the transition from steady to time-dependent flow conditions. For $\text{Ra}\approx\text{Ra}_c$, $\tau_0\gg\tau_t$ and the thermal diffusion smoothes any perturbation well before one revolution, whereas for $\text{Ra}>\text{Ra}_c$, $\tau_0<\tau_t$ and the perturbations have time to propagate into the entire flow field allowing instabilities to occur. For increasing Rayleigh number, τ_0 decreases, so that this situation holds more easily. In the limit $\text{Ra}\gg\text{Ra}_c$ it is [using relations (1) and (4)]:

$$\tau_0 \approx [\text{Ra}_c(\tau_t/\tau_v)]^{1/2}\tau_g. \tag{5}$$

The behavior of hot and cold thermal perturbations is summarized as follows (Gollub and Benson[13]): for small Prandtl numbers the thermal diffusion smoothes perturbations very rapidly because of Eq. (2). Simultaneously, from Eq. (3), a thermal disturbance will propagate with a timescale equal to τ_v that will be very long in comparison to τ_t: therefore, from Eq. (4), if the Rayleigh number is larger than Ra_c, it is $\tau_0<\tau_t$ and the system moves into the transition region where instabilities start to dominate. The opposite happens for high Prandtl and low Rayleigh numbers.

The mechanisms of motion of thermal perturbations were studied by Welander[1] in his 1D model (pipe loop). The stationary solution consists of a uniform temperature into each half side of the pipe. This solution becomes unstable for increasing values of the temperature difference. Instabilities are connected to regions whose temperatures are different from those of the surrounding fluid: these flow regions are embedded into the mean flow. Weak and strong instabilities are encountered: the first kind are impulsive and keep the same sign during the motion, while the second are oscillatory and are associated with flow reversal. The latter are usually investigated in greater detail because they allow temperature anomalies (hot and cold blobs) to form and to travel along

the pipe. They induce accelerations and decelerations of the fluid if $\tau_0 < \tau_t$ as in Eq. (4). For example, suppose a blob is heated near the heating element: it accelerates toward the upper cold region (where the velocity takes the maximum value) and therewith it decelerates toward the lower hot region (where the velocity is minimum). Therefore, the timescale for heating is much higher than that for cooling: the blob conveys momentum at each revolution producing oscillations. As a consequence, a feedback process takes place: the presence of a blob enhances oscillation and oscillations increase the blob intensity. The mechanism is similar for cold blobs.

The transition to the turbulent regime is influenced not only by the Rayleigh and Prandtl numbers, but also by the geometry of the vessel. Desrayaud and Lauriat[10] performed a numerical simulation to emphasize that instabilities of the main flow occur only when the width of the vessel is decreased to a size two or three times its height: the two rolls are stable even for high Rayleigh numbers. To this end, the fundamental parameter is the aspect ratio A ($A = L/H$, where H and L are the height and width of the vessel). It was observed that, for $A \approx 10$ or more, the flow field consists of two steady counterrotating vortices: this condition continues for high Rayleigh numbers as well. For $A \approx 2$ the two vortices start to oscillate: Busse[14] estimated the oscillation period to be roughly equal to the revolution time of a particle along one of the vortices. The beginning of the oscillating regime is understood within the analysis of the characteristic propagation $\tau_d(3)$ and revolution timescales $\tau_0(4)$. The analysis of these timescales reveals that, when the aspect ratio is low (say smaller than 15), $\tau_0 \ll \tau_d$ (instability) and the blobs preserve their temperature difference in comparison with the surrounding fluid. The flow configuration approaches stability ($\tau_0 > \tau_d$) for values of A larger than approximately 20.

While the flow behavior is quite well understood at low Rayleigh numbers, this is not the case for high Rayleigh numbers. In this situation, several hot (or cold) blobs are simultaneously present in the vessel (Bolton et al.[8]). A multiline power spectrum is obtained from the time history of one velocity component (or of the temperature), due to the interaction between traveling blobs and oscillations of the counterrotating vortices. This suggests that more than one perturbation mechanism is simultaneously present in the flow field. Nevertheless, the physical origin of these perturbations is not completely understood.

Whenever the heating element is placed over the bottom wall and not exactly on it, a region of stable stratification is observed on the bottom part of the vessel. It acts as an harmonic oscillator of frequency N_{BV}. Desrayaud and Lauriat,[10] in their numerical simulation, located the heating element at about 1/3 of the vessel height: they noticed a second line in temperature and velocity spectra at about $f/10$ (where f is the main spectral line connected to oscillations of the convective rolls). In the present experimental conditions, the heating channel is placed just on the bottom wall, so that this frequency component is not expected.
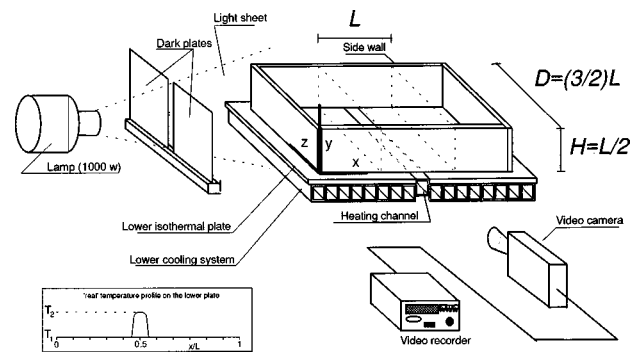

FIG. 2. Experimental setup, frame reference, and temperature boundary condition (measured using a thermocouple) on the lower plate. The length is $L = 12$ cm. The lower plate cooling system is shown (the upper cooling system is not shown and is similar except for the heating channel).

III. EXPERIMENTAL CONDITIONS AND MEASUREMENT TECHNIQUES

The convection is generated in a rectangular vessel filled with a water-glycerol mixture (from 0% to about 7.5% in volume of glycerol) (Fig. 2). The side walls of the vessel are adiabatic (made of perspex): to provide insulation, they are surrounded by water chambers (indicated by dotted lines in Fig. 2). The upper and lower surfaces are isothermal aluminum plates (thickness equal to 0.5 cm) kept at the same constant temperature. This temperature is determined by the temperature of the water flowing inside nearby channels (connected to the aluminum plates) having square cross section (size equal to 2 cm, thickness ≈ 2 mm) (Fig. 2). The linear heating element is made by one of these channels placed inside the center of the lower plate and insulated from it by a silicone layer (thickness ≈ 2 mm). The transverse dimension of the channel is equal to $L/6$ (where $L = 12$ cm is the inner width of the vessel) and it extends over the whole length D of the vessel ($D = 3/2L$). The heating is supplied by hot water flowing inside the channel controlled by a thermostat (error equal to ± 0.1 °C): The real temperature profile inside the vessel was controlled by a thermocouple and is also shown in Fig. 2. The x axis is taken along the width of the vessel (orthogonal to the linear heating channel), the y axis is directed in the vertical, and the z horizontally (parallel to the heating channel). The aspect ratio is $A = L/H = 2$. The control parameter, i.e., the Rayleigh number, is based on the temperature difference between the water into the heating channel and the water in the channels connected to the isothermal plates. In the present experiment the Rayleigh number ranges from 1.7×10^6 up to 1.7×10^7: the average fluid temperature inside the vessel is equal to about 15 °C. The critical Rayleigh number, Ra_c, was estimated by measuring the time for revolution $\tau_0(4)$ (Table I): it is $Ra_c \approx 1300$ and

TABLE I. Optical and flow parameters ($\Delta T = 1.9$ °C, $T \approx 15$ °C in pure water).

Intersection angle (degrees)	6
Volume dimensions x, y, z (mm)	0.12, 0.12, 1.03
Fringe spacing (μm)	6.4
Time integral scale (s)	180

TABLE II. Flow timescales (in seconds) for the water-glycerol mixtures at $\Delta T = 1.9\,^\circ\text{C}$ ($T \approx 15\,^\circ\text{C}$). The kinematic viscosity, thermal diffusivity, and thermal expansion of the mixtures are computed from Chemical Handbooks (at different temperatures).

	0%	2.5%	7.5%
Thermal diffusion time scale (τ_t)	7.2×10^3	7.2×10^3	7.5×10^3
Viscous diffusion time scale (τ_v)	3.0×10^3	2.7×10^3	2.2×10^3
Time scale for buoyancy (τ_g)	3.5	2.3	2.0
Propagation time scale (τ_d)	8.0×10^3	8.0×10^3	8.1×10^3
Revolution time scale (τ_0)	1.9×10^2	2.1×10^2	6.2×10^2

hence $\text{Ra}/\text{Ra}_c \approx 1.4 \times 10^3$, corresponding to strongly established instabilities. However, the flow motion is still dominated by large scale organized structures (weakly chaotic flow). The average Prandtl number is around 5 and it is dependent on the water-glycerol mixture: the different mixtures are selected mainly to point out the effect of Prandtl number on the flow behavior. For each mixture kinematic viscosity, thermal diffusivity and thermal expansion coefficients are derived as functions of the temperature. In Table II the timescales for the different water-glycerol mixtures are given. They are computed from the geometry of the vessel, the temperature difference, the thermal expansion coefficient, the thermal diffusivity, and the kinematic viscosity. These last three quantities are dependent on the concentration of glycerol and on the temperature. For each concentration and temperature they are computed from Chemical Handbook by using linear interpolation between the values given each 5 °C in temperature and every increment of 5% in concentration.

For low Rayleigh number the flow configuration is basically 2D. However, especially at large Rayleigh number (larger than 5×10^6 for pure water), some meandering motion (along the heating channel) is also observed. Nevertheless, even at these Rayleigh numbers, the analysis of long trajectories of seeding particles reveals that they remain on the same plane for more than 5 min (about 2 integral timescale). This suggests that the flow nature is mostly planar or at least that the timescales for the velocity component orthogonal to the light plane are larger than those of the in-plane velocity components.

A. Setup for LDA measurements

The horizontal velocity component (along x direction) is measured with an LDA system in the forward scatter optical configuration. The horizontal component is selected over the vertical due to the vanishing mean value: the change in the sign of the velocity more easily allows the detection of the oscillations. A 25-mW He-Ne laser is used as coherent light source. The main optical parameters are summarized in Table I. A double Bragg cell is used to detect the direction of the velocity and to increase the resolution of velocity measurements (the maximum velocity being below 1 cm/s).

The measurement volume is placed above the heating channel ($x = L/2$, $z = D/2$) at two-thirds of the vessel height ($y = 2/3H$). To avoid random fluctuations of the laser beams, due to local changes of refractive index, the temperature difference is never higher than 15°. Styrene particles with mean size equal to 5 μm are used as seeders. The Doppler signals are bandpass prefiltered and then acquired and processed by an IFA 550: the mean data rate is over 200 Hz.

The error on each velocity measurement is mainly determined by the error on the evaluation of the angle between the laser beams and it is equal to 0.5%: this is a bias error affecting only the absolute value of the velocity. If relative velocities are computed, the error is reduced to the error in the evaluation of the Doppler frequency introduced by the signal processor (about 0.3%).

The analog output is sampled at constant frequency (about 15 Hz) by using a suitable acquisition card and software: this corresponds to a zero-order interpolation (hold and sampling method). A ''step'' noise is introduced for hold and sampled signals (Adrian and Yao[15]): it is sensed at frequencies higher than $\dot{N}$ ($\dot{N} = 15$ Hz is the sampling frequency), that is, well above those of interest for the present study. The hold and sampling method avoids bias errors on velocity measurements if the sampling frequency is less than 5–10 times the processor data rate, as in the present measurements. Moreover, the mean data density, $N_D = T_i f_D$ (where T_i is the integral timescale and f_D is the valid data rate) is higher than 1000, that is well above the threshold value $N_D = 20$ indicated by Benak et al.[16] as a minimum for avoiding bias errors.

About 10^5 samples are collected for each value of the control parameter. A further low-pass filtering (below 1 Hz) is applied on the acquired data to smooth small scale fluctuations and to handle a small number of samples in the computations. The total acquisition time is about 40 T_i (2 hours). Conventional algorithms are applied to the equispaced data to compute correlation and spectral density functions.

Among the wide variety of tools for signal decomposition, it is necessary to choose those which emphasize the requested flow features. In this paper, the decomposition based on the Wavelet Transform (WT) is used (Farge[19]). The wavelet analysis is used in time rather than space: therefore, it is equivalent to the use of Fourier analysis by constant percentage bandwidth Gaussian bandpass filters. The 1D Morlet complex wavelet is employed. The WT clearly points out the variation of the fundamental frequencies for increasing values of the control parameter (the Rayleigh number) and therefore contributes to clarify the underlying mechanisms leading to the instabilities.

B. Setup for PTV measurements

The two velocity components on the (x,y) plane, orthogonal to the heating channel, are measured by means of PTV. The technique is based on image analysis and gives a description of the time evolution of the whole velocity field. A 1000-W Arc Lamp continuously illuminates the test section (through a slot) generating a 1-cm-thick light sheet orthogonal to the heat channel and placed at middle depth of the vessel ($z=D/2$). The working fluid is seeded with small, nonbuoyant particles, 50 μm in diameter. A video camera (shutter 1/25 s), orthogonal to the light sheet, takes series of images which are stored on tape by a S-VHS video recorder (frame rate 25 Hz). Then, one frame out of four is digitized at a 512×512 pixel resolution and processed to individuate the locations of the seeding particles (which on the average occupy 4÷5 pixels). The successive locations of the particles on different frames are elaborated by a tracking algorithm in order to recognize the trajectories.

Velocity samples are obtained from particle displacements along trajectories at given time intervals. The tracking algorithm is based on two parameters: a maximum velocity and a maximum acceleration. Typical values of these parameters during the present experiment were, respectively, 20 pixel/frame and 5 pixel/frame[2]. This means that the particle displacement between two frames is not expected to be larger than 20 pixels. Since particle locations are known with the precision of 1 pixel, the relative error is around 5%. It could be useful to notice that this error is much higher for the horizontal velocity component because the average displacement along the horizontal is lower than that along the vertical.

The velocity field on a regular grid is obtained by inverse distance interpolation. As a result, two components of the velocity are known on a grid with 23 cells along the horizontal and 15 along the vertical at 6.25-Hz rate. The total number of cells is selected to have at least one sample in each grid point: therefore, the interpolation relative error is lower than 5% (Agüi and Jimenez[17]). A similar error is obtained also by using the error diagrams of Spedding and Rignot.[18] Results are averaged over about 30 images, (5 s), which is small enough compared to the integral timescale of the phenomenon (about 0.03 T_i). The total acquisition time is about 10 T_i (1/2 h).

IV. RESULTS AND DISCUSSION

The timescales, defined in Secs. I and II, are computed in Table II for the different water-glycerol mixtures: the revolution timescale is obtained from LDA spectral measurements and it is used to compute Ra/Ra$_c$. These timescales are computed by using different values for the kinematic viscosity, thermal diffusivity, and thermal expansion coefficient for each mixture and for each temperature. The flow exhibits an oscillation characterized by a decreasing period as the Rayleigh number increases. In the following, LDA and PTV results will be outlined separately.
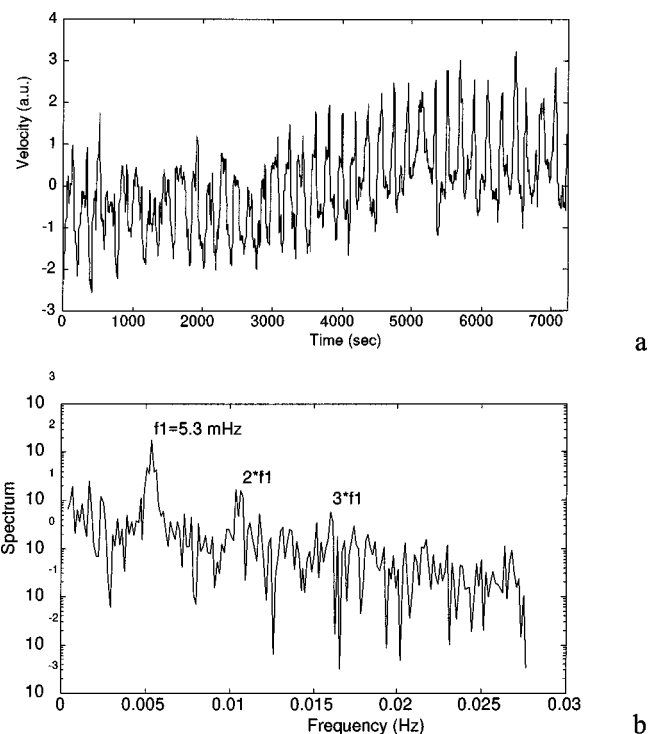

FIG. 3. Time history (a) and power spectrum (b) of the horizontal velocity component at point ($x=L/2$, $y=2/3H$, $z=D/2$): Ra$=1.7\times10^6$ ($\Delta T=1.9\ ^\circ$C), Pr$=2.5$. Pure water.

A. Results of LDA measurements

The measurements start at a Rayleigh number equal to 1.7×10^6 ($\Delta T\sim1.9\ ^\circ$C) where the flow behavior is time dependent (Fig. 1): A thermal plume raises from the heating channel and produces regular oscillations of two counterrotating vortices toward the left and right hand side of the vessel. In Fig. 3 the time history and the power spectrum of the horizontal velocity component for pure water are shown. A line at $f_1\approx(5.3\pm0.14)$ mHz, corresponding to the oscillation of the vortex pattern in time, and its harmonics are detected: this main frequency is very close to the inverse of the revolution timescale (as noticed by comparing to Table II). It can be also observed a low frequency oscillation of the signal over the entire time interval: it corresponds to the inverse of the total acquisition time. This indicates that there is a long period oscillation (about 40 revolutions) in which the horizontal velocity moves from a negative mean value (thermal plume slightly inclined toward the left) to a positive mean value (plume inclined towards the right). This behavior does not derive from laser or lamp heating because it is still observed when they are switched off. Moreover, in repeated experiments, there is no preferred direction of inclination, and the plume starts equally on both the left and right hand side of the vessel. Thus when the temperature difference is low, the bias toward one side of the vessel and the oscillation of this configuration is a stable initial condition for the thermal plume.

When the Rayleigh number increases, the horizontal velocity component shows sudden changes from a state of almost regular oscillations (characterized by a single fre-
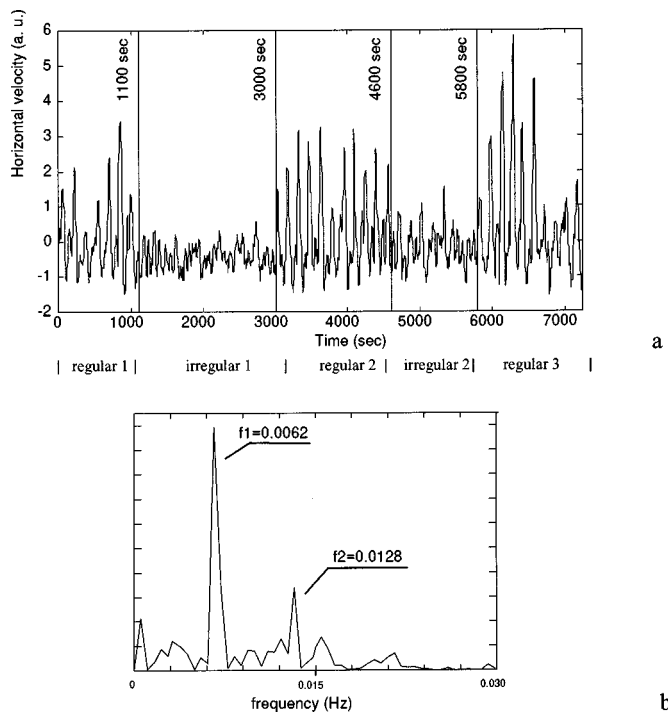
FIG. 4. Time history (a) and power spectrum (b) of the horizontal velocity component at same point of Fig. 3: Ra$=2.3\times10^6$ ($\Delta T=2.6\,°$C), Pr$=2.4$. Pure water.

quency) to a state of irregular oscillations (characterized by more than one frequency). Those conditions alternate randomly in time. The situation for Ra$=2.3\times10^6$ is given in Fig. 4(a): the irregular phases have durations similar or even larger than the regular phases. The power spectrum is given in Fig. 4(b). The main line is $f_1=(6.20\pm0.14)$ mHz and it is mostly observed during the regular phase. On the other hand, the second line is mainly detected during the irregular phase (together with the main one): it is close to twice the main one. Specifically, the second frequency is $f_2=(12.87\pm0.14)$ mHz, and the ratio is $f_2/f_1\approx(2.06\pm0.10)$. It is interesting to note that, while during the irregular phase the mean value is negative (plume inclined towards the left), during the regular phase it is positive (plume inclined towards the right): in both cases oscillations take place in a nonsymmetrical way.

For a further increase in Rayleigh number the regular and irregular intervals are characterized by two incommensurate frequencies f_1 and f_2. At Ra$=3.7\times10^6$ the frequency of the regular phase is $f_1=(7.9\pm0.14)$ mHz whereas that of the irregular is now far from $2f_1$ [it is $f_2=(18.1\pm0.14)$ mHz and $f_2/f_1\approx2.29\pm0.05$] (Fig. 5). The coupling between the two frequencies is confirmed by the peak broadening around f_1 and f_2 [Fig. 5(b)]. However, in contrast to pure quasi-periodic transition (as that observed by Gollub and Benson[13]), the two frequencies alternate in time rather than occur simultaneously. In Figs. 5(c) and 5(d) this is shown for irregular (II) and regular (III) time windows. The presence of the linear heating channel (instead of the conventional uniform heating from below) leads the system into a transition regime characterized by the intermittency between different flow configurations.

This sequence of regular and irregular phases is observed in dynamical systems when the transition to chaotic regimes takes place via the intermittency scenario. Three types of intermittency have been reported (Bergé et al.[20]). In type I intermittency regular phases are characterized by one main frequency, whereas those irregular do not show any dominant frequency. The amplitude is almost constant when moving from one phase to the other and the probability distribution of the lengths of phases has the maximum moved toward large values. Type II intermittency shows different amplitudes between the regular and irregular phases: the two are characterized by different and incommensurate frequencies. The distribution of lengths of the phases has the maximum at small values and extended exponentially toward very large values. Type III intermittency is very similar to type II concerning amplitude and distribution of interval lengths. However, the spectrum of the irregular phases contains subharmonics of the main frequency of the regular phases (Manneville and Pomeau[21]). The observed data do not show subharmonics between the two phases, but rather different and incommensurate frequencies and support the selection of type II intermittency as responsible for the transition. However, the detection of subharmonics is usually very difficult due to their small amplitude compared to the background noise. Therefore, in the present experiment, transition via type III intermittency cannot be ruled completely out expecially at small Rayleigh number (for which the ratio f_2/f_1 is close to 2).

The frequency contribution at each instant and the lengths of the phases are determined by using the modulus of WT. In Fig. 6(a) this operation is performed for Ra$=4.3\times10^6$: a low frequency (about 7 mHz) is observed throughout all the acquisition interval (regular phases), but sometimes a second frequency (about 17 mHz) appears. In Fig. 6(b) the number of intervals of given length for this second frequency is shown: the distribution has a very long tail (the maximum length is 32 s, while the minimum is 2 s) toward large intervals as predicted for type II and III intermittency.

In performing the present analysis, the determination of the instant when the flow changes the frequency of oscillation and the selection of the main and other lines in the power spectrum are crucial: to avoid arbitrariness, the WT tool is employed. It enables to detect changes from one oscillatory regime to another: this is pointed out in the wavelet modulus at all scales. In Fig. 7(a) an example is shown by using the modulus of WT for the 7.5% water-glycerol mixture at Ra$=6.8\times10^6$: so far, instants of frequency change are detected. To distinguish between main and other lines in the power spectrum, a threshold criterion is applied in order to detect the two main frequencies [in the case of Fig. 7(b) $f_1\approx12$ mHz and $f_2\approx26$ mHz].

The ratio of the main frequency detected during the irregular phases to that during the regular phases, f_2/f_1, was computed for the three water-glycerol mixtures at different Rayleigh numbers. In Fig. 8 such a ratio is plotted. As the Rayleigh number increases, the ratio starts from about 2 (commensurate frequencies), increases to about $2.3\div2.4$ (incommensurate frequencies) and returns close to 2. This seems to indicate that there is a route from a transition sce-
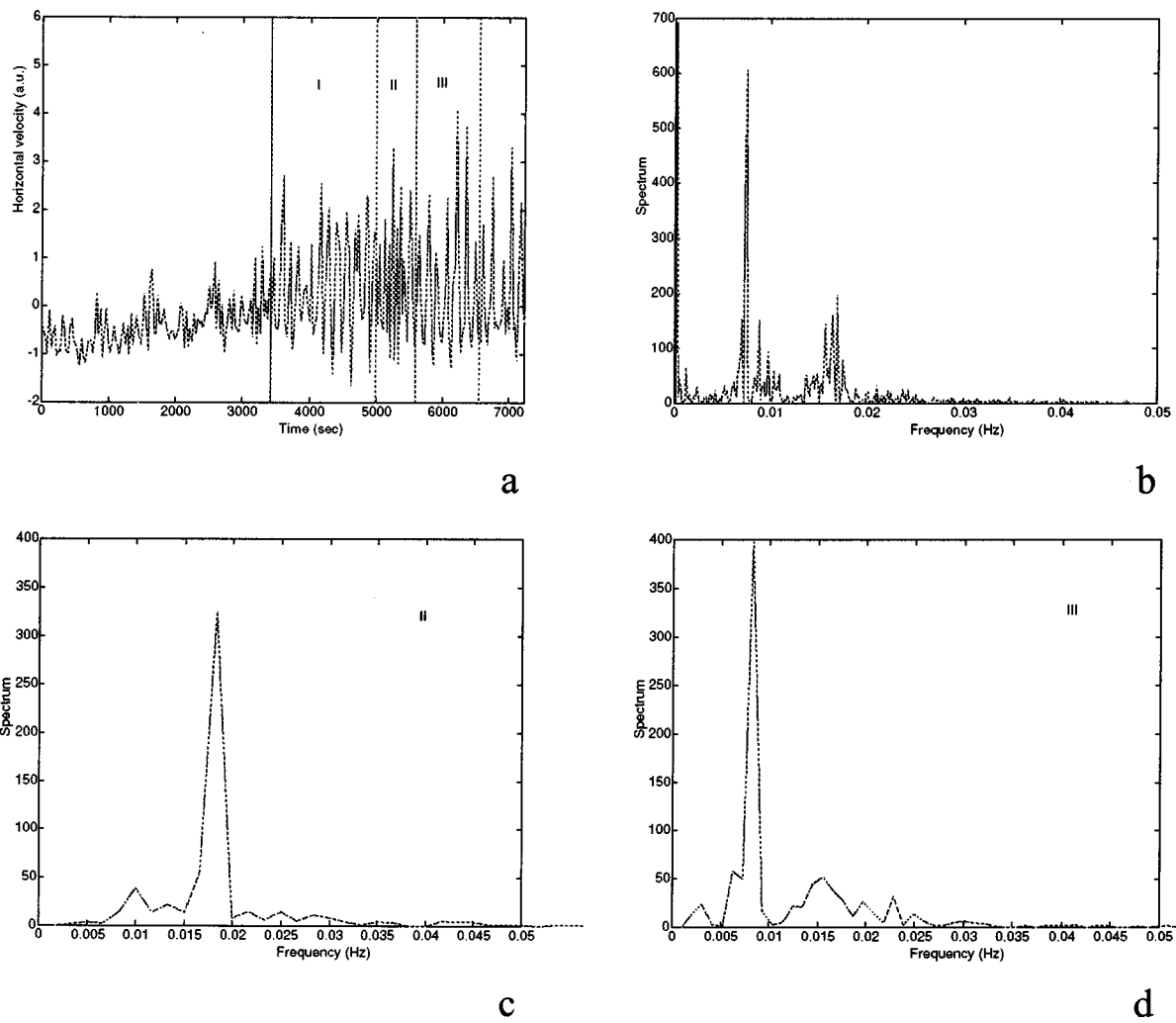
FIG. 5. Time history (a) of the horizontal velocity component at same point than Fig. 3. Power spectrum of the whole time history (b), of the window II (c) and III (d): Ra=3.7×10^6 (ΔT=4.3 °C), Pr=2.3. Pure water.
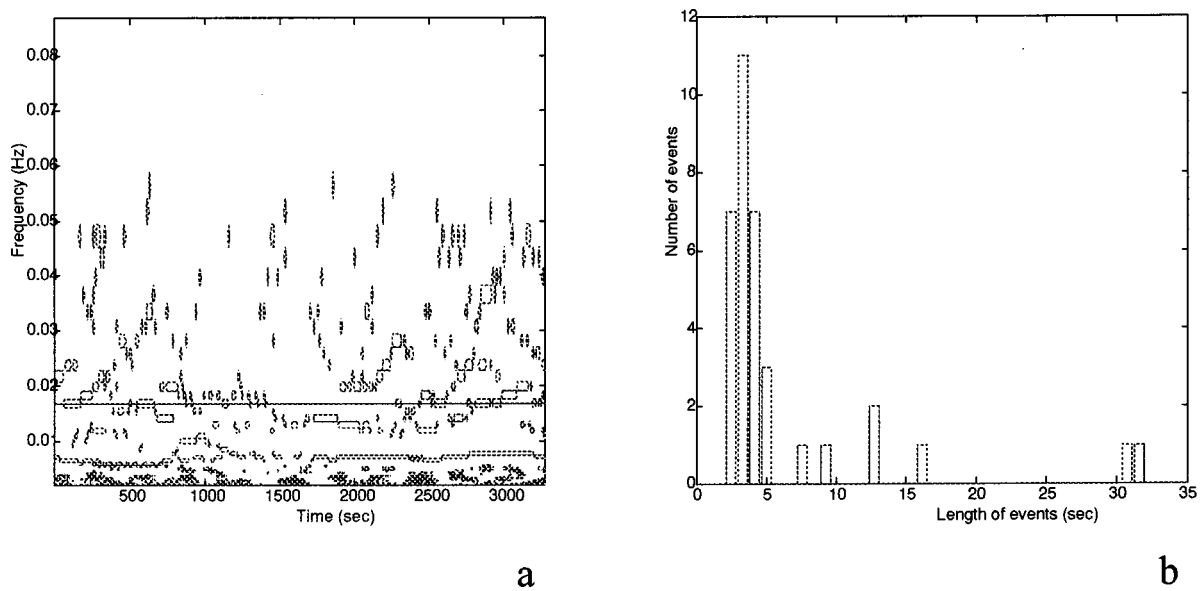

FIG. 6. Modulus of WT (a) and distribution of time interval duration at the frequency 0.017 Hz with intensity larger than 5% of the maximum (b). Water-glycerol 2.5% mixture at Ra=4.3×10^6.
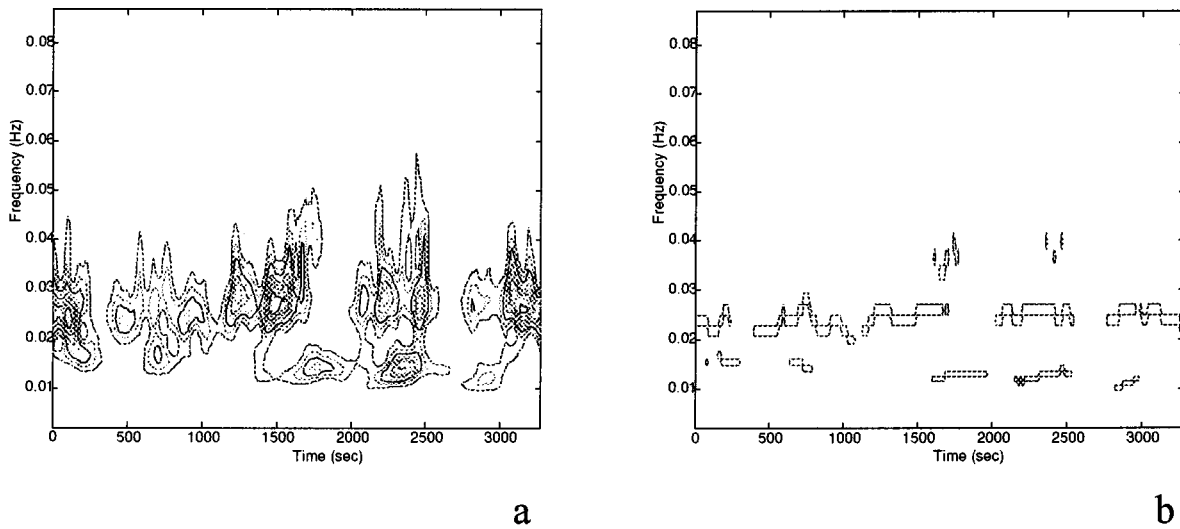
FIG. 7. Modulus of WT (a) and local maxima over 15% of the absolute maximum (b). Water-glycerol mixture at 7.5% with $Ra = 6.8 \times 10^6$.

nario based on type III intermittency to another based on type II intermittency. The observed trend of increasing and successive decreasing of f_2/f_1 is similar for the three mixtures, although delayed to high Rayleigh numbers as the percentage of glycerol becomes larger. The differences between the mixtures will be outlined in the next paragraphs: here, it should be noticed that the percentage of glycerol mostly modifies the viscous diffusion and buoyancy timescales rather than the thermal diffusion timescale (Table II). Therefore, the revolution time scale (τ_0) is much higher for the 7.5% mixture than for pure water, whereas the timescale for propagation (τ_d) is about the same (Table II). This can be obtained from Eqs. (3), (4), and (5) in Sec. II. Following indications given in that section, the 7.5% mixture is more stable than the pure water at a given Rayleigh number.

The detected frequencies increase as the Rayleigh number. Busse and Whitehead[7] pointed out that the period of oscillatory convection has a general $Ra^{-2/3}$ dependence: Therefore the frequency must increase as $Ra^{2/3}$. This law was confirmed both numerically and experimentally (Clever and

Busse[9]). In Fig. 9 the variation of the nondimensional frequencies ($f^* = f\tau_t$, using the thermal diffusion timescale τ_t) with Rayleigh number is shown: only the main frequencies (determined by WT) are shown. The data from the 7.5% mixtures are often higher than the others: this could be due to the slightly larger values of τ_t for such a mixture (Table II). The data follow a $Ra^{0.5}$ law that is lower than theoretical predictions 2/3, but very close to the power law obtained from Eq. (4) when $Ra \gg Ra_c$. The trend toward a lower Rayleigh number dependence was observed previously for $Ra > 10^6$ (Busse and Whitehead[7]). Desrayaud and Lauriat[10] noticed that this power law is slightly affected by the aspect ratio A. As pointed out by Busse and Whitehead,[7] the dimensionless frequency f^* should not depend on the Prandtl number ($Pr \geqslant 1$). However, a slight Prandtl number dependence is usually observed.

To investigate in greater detail how the frequency is dependent on Rayleigh and Prandtl number, suitable time scales must be used. By examining Eqs. (1) and (2), it can be seen that the dimensionless frequency f' ($f' = f\tau_g$, where τ_g
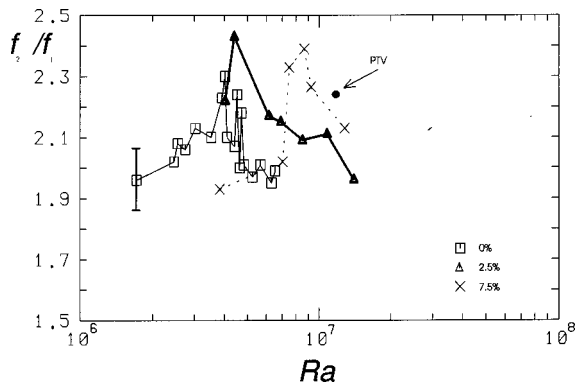

FIG. 8. Variation of the ratio between the frequency of the irregular (f_2) and regular (f_1) phases with Rayleigh number. Symbols show different water-glycerol mixtures. The error is indicated by the vertical bar. The point obtained from PTV measurements is labeled.
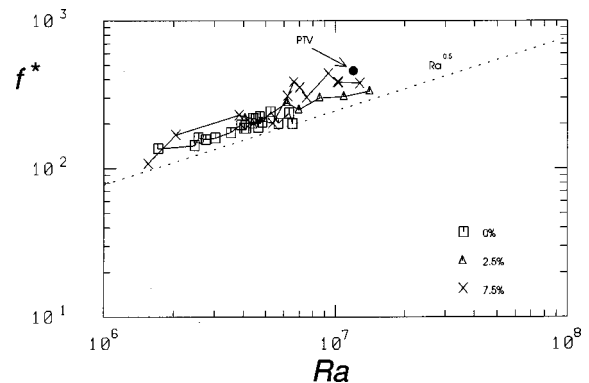

FIG. 9. Variation of main frequencies with Rayleigh number. The dimensionless frequency ($f^* = f\tau_t$) is used. Symbols show different water-glycerol mixtures. The line $Ra^{0.5}$ is also shown. The point obtained from PTV measurements is labeled.
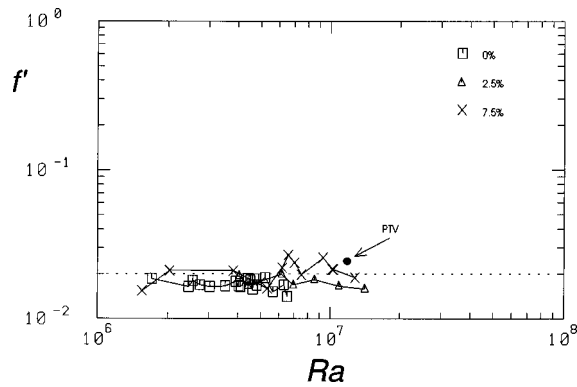
FIG. 10. Variation of main frequencies with Rayleigh number. The dimensionless frequency ($f' = f\tau_g$) is used. Symbols show different water-glycerol mixtures. The point obtained from PTV measurements is labeled.

is the timescale for buoyancy) has a very slight dependence on Rayleigh number. By definition $f' \approx f^* \mathrm{Ra}^{-0.5} \mathrm{Pr}^{-0.5}$, so taking the present $f^*(\mathrm{Ra})$ dependence (0.5), one finds $f' \approx \mathrm{Pr}^{-0.5}$, i.e., independent on Rayleigh number. In Fig. 10 the variation of f' with Ra is shown for the main lines in the power spectrum: data are observed to have a very slight dependence on Ra over the whole range of Rayleigh numbers. Even in this case the 7.5% mixture attains the higher values: however, for such a mixture the timescale for buoyancy is lower than for the others, so that a difference in timescale cannot explain the observed behavior. To do this, the change in Prandtl number between the different mixtures must be considered. On average, the Prandtl number of the 7.5% mixture is about 1.5 times larger than that of pure water. To take into account this effect, the correct dimensionless frequency is $f'' = f\tau_v$ (where τ_v is the viscous diffusion timescale). In Fig. 11 such a frequency is shown versus the Rayleigh number. The difference between the different mixtures almost completely disappears, so that this selection points out the inherent flow behavior. The expected variation with Rayleigh number is given by $f'' = f\tau_v = f^*(1/\mathrm{Pr}) \approx \mathrm{Ra}^{0.5} \mathrm{Pr}^{-1}$ and the observed data reasonably follow a $\mathrm{Ra}^{0.5}$ dependence consistently with previous findings.

The variation of main and secondary dimensionless frequencies (f^* and f') and their linear combination are shown
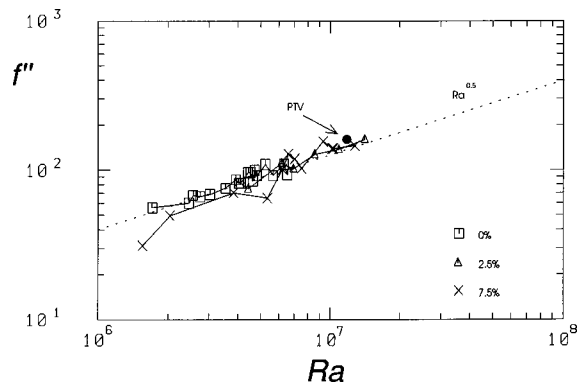

FIG. 11. Variation of main frequencies with Rayleigh number. The dimensionless frequency ($f'' = f\tau_v$) is used. Symbols show different water-glycerol mixtures. The point obtained from PTV measurements is labeled.
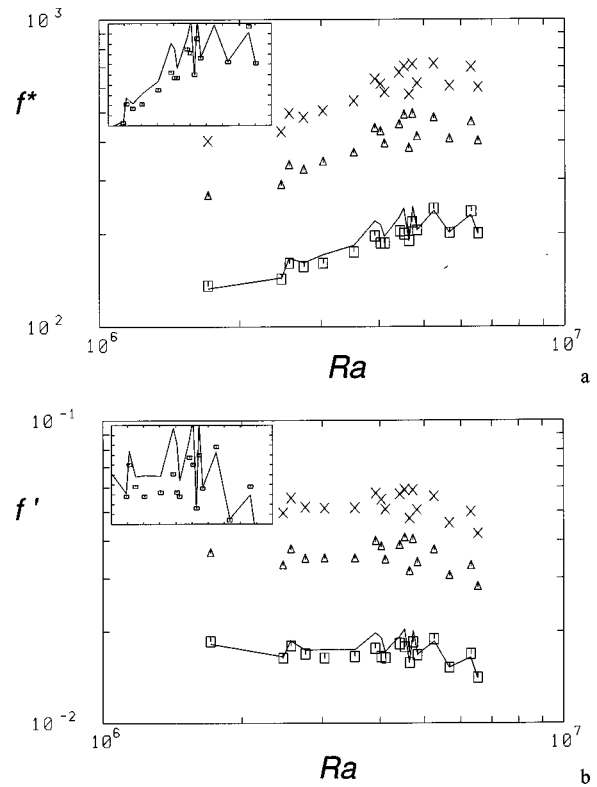

FIG. 12. Variation of dimensionless frequency $f^* = f\tau_t$ (a) and $f' = f\tau_g$ (b) with Rayleigh number for pure water. The two main frequencies f_1 ($\square$), f_2 ($\triangle$), and their sum $f_1 + f_2$ ($\times$) are plotted. The continuous lines indicate $f_2/2$. In the boxes the frequencies f_1 and $f_2/2$ are emphasized on a linear plot [the horizontal axes are from 2×10^6 to 7×10^6, whereas the vertical axis is from 140 to 240 in (a) and from 0.015 to 0.020 in (b)].

in Fig. 12 for pure water. Three distinct regions are separated (f_1, f_2, and $f_1 + f_2$) indicating that the whole set of acquired data well reproduce a transition scenario based on two frequencies intermittently observed in time. As already noticed, for small Rayleigh numbers the frequency f_1 is close to $f_2/2$ (also given in Fig. 12), whereas for increasing Rayleigh numbers the two frequencies are incommensurate (see small boxes in Fig. 12). They correspond to different oscillation modes of the two convective rolls. Such modes can be related to the spatial flow configurations into the vessel and this point will be clarified by PTV measurements.

B. Results of PTV measurements

The velocity measurements by PTV are performed on almost instantaneous fields in comparison to the integral timescale of the flow. Several seeding particles are tracked for a time interval in the order of the integral timescale: this means that they remain into the laser sheet (2D motion) for long time intervals. This is true even at high Rayleigh number.

By superimposing the images collected during the whole acquisition, it is possible to obtain the mean flow field: of course this is indicative only of the average motion. In Fig. 13(a) the mean flow field averaged over about 1800 s is shown. As predicted, the mean flow configuration consists of two counterrotating vortices which occupy the whole vessel:
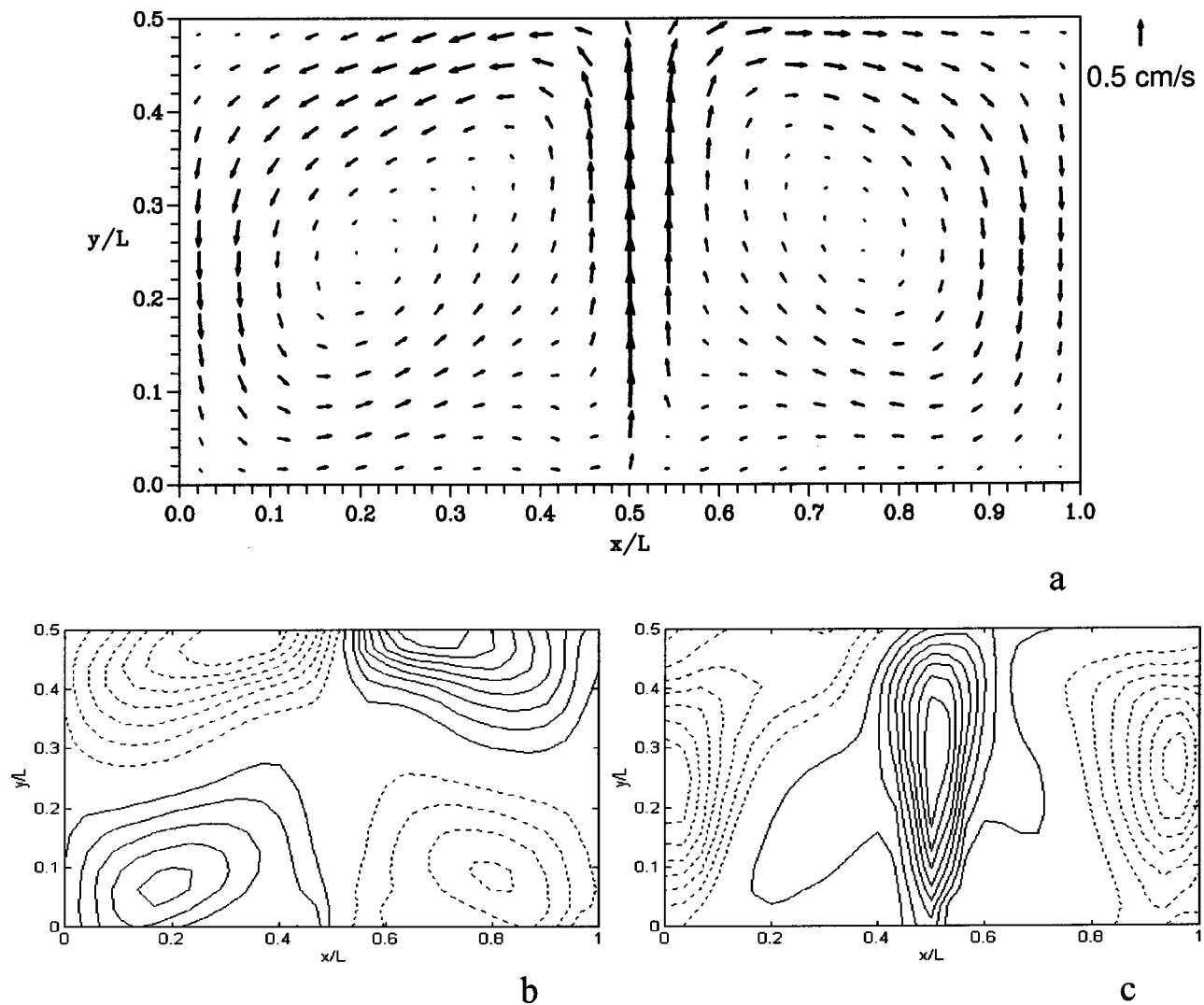
FIG. 13. PTV measurements: average velocity field (a). Dimensionless x and y are used ($L = 12$ cm is the width of the vessel). The maximum velocity is about 1 cm/s, Ra$= 1.2 \times 10^7$. Water-glycerol 7.5% mixture. Isolevels of horizontal (b) and vertical velocity (c) components: positive (continuous lines) and negative (dotted lines).

The velocity is higher near the center where the heating channel is located. The flow configuration is highly symmetric as confirmed by the isolevels of horizontal and vertical velocity components given in Figs. 13(b) and 13(c): The horizontal velocity component separates the vessel into four quadrants with the same sign along the diagonal, whereas the vertical component into three bands with positive sign at the center and negative sign on both left and right side. In the following only iso-vertical velocity contours will be shown: they retain the differences between right and left side of the flow field better than the horizontal. However, the fundamental frequencies are observed both in the horizontal and in the vertical components. In Fig. 14 four instantaneous consecutive fields are presented. It is possible to recognize and to follow a region with velocity considerably higher than in the neighbors (blob): it moves upward, then deviates on the right and returns downward. Simultaneously, a new blob moves upward and deviates on the left. This is essentially the basic mechanism that gives the main peaks in spectra from LDA

measurements: the velocity components at a point oscillate in time.

Due to the large timescales of this flow field, it is even possible to perform spectral analysis on PTV data. Time histories of the two velocity components are obtained at each point of the field. In Fig. 15, the spectra of horizontal and vertical velocity components, at the same point of LDA measurements, are shown: the Rayleigh number is 1.2×10^7 and the Prandtl number is about 3. The 7.5% water-glycerol mixture is employed. The main line for the horizontal velocity component is $f_1 = (17.0 \pm 0.5)$ mHz, resulting in $f_1^* = f_1 \tau_t = 460$, $f_1' = f_1 \tau_g = 0.026$, and $f_1'' = f_1 \tau_v = 150$. These values are plotted in Figs. 9, 10, and 11 together with the LDA results and good agreement is observed. A very small second line is observed at about 38.5 mHz. The spectrum of the vertical component shows the same main line as the horizontal, a second line at about 6 mHz (which is connected to a fluctuation in only one time interval as will be shown in the
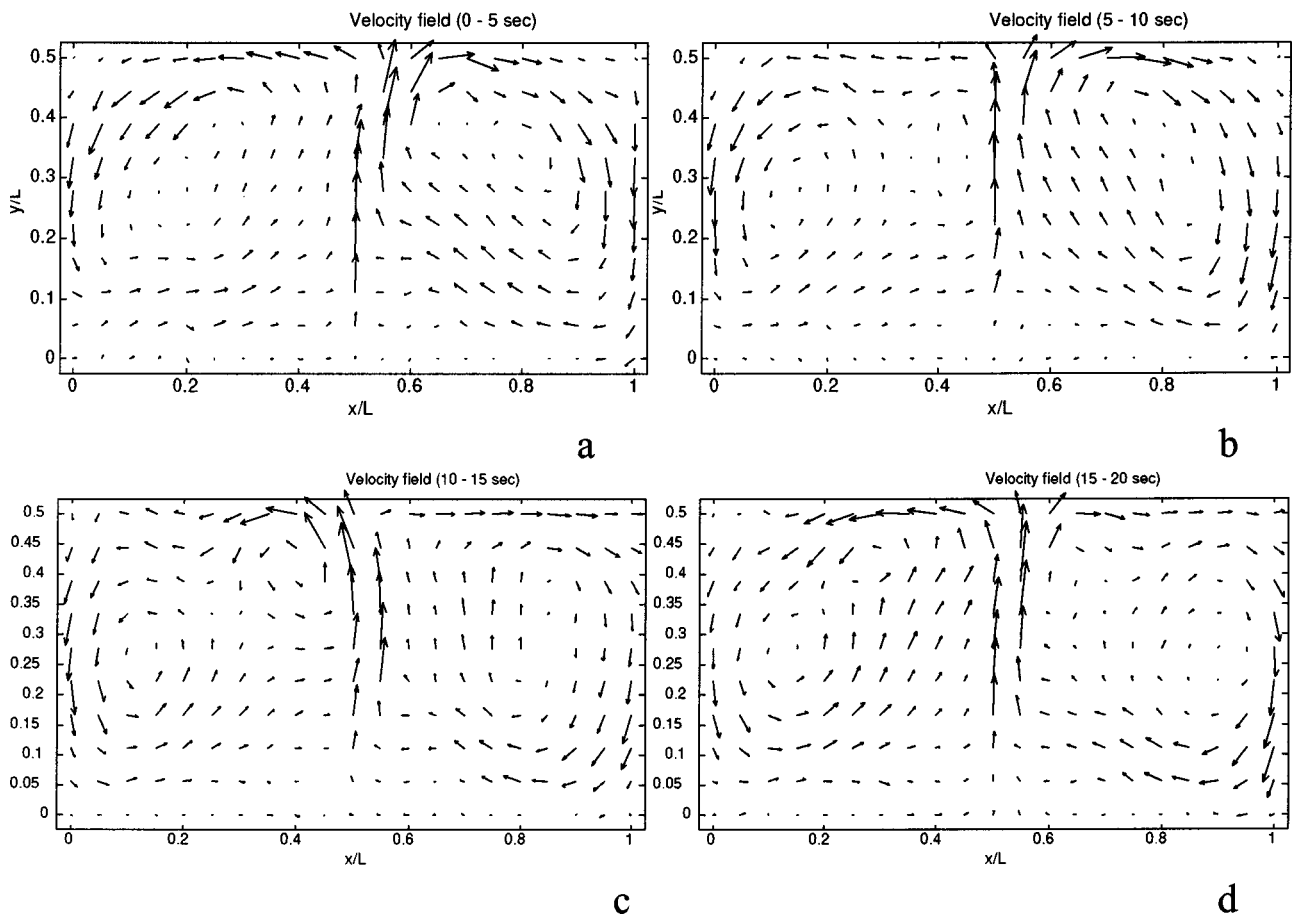
FIG. 14. Four instantaneous consecutive velocity fields: $Ra = 1.2 \times 10^7$. Water-glycerol 7.5% mixture.

following), a third line at about 38.5 mHz, and another at about 34 mHz. This last one is related to the harmonic $2f_1$, whereas the third one at the frequency f_2: the ratio $f_2 / f_1 \approx 2.25$ is given in Fig. 8 and it is in agreement with the results obtained by LDA.

The comparison between the two velocity components reveals a picture different from that expected by the flow fields of Figs. 13 and 14. For such an oscillating plume, the horizontal velocity is expected to change sign during one

oscillation of the plume: therefore, one oscillation of the horizontal velocity occur during one oscillation of the plume. Conversely, the vertical velocity holds the same sign during one oscillation of the plume, so that two oscillations occur within the same time interval. As a result, the vertical component should display a period of oscillation equal to 1/2 that of the horizontal and its spectrum should exhibit a frequency twice than that of the horizontal. This happens when the plume oscillates symmetrically. If the symmetry axis is dis-
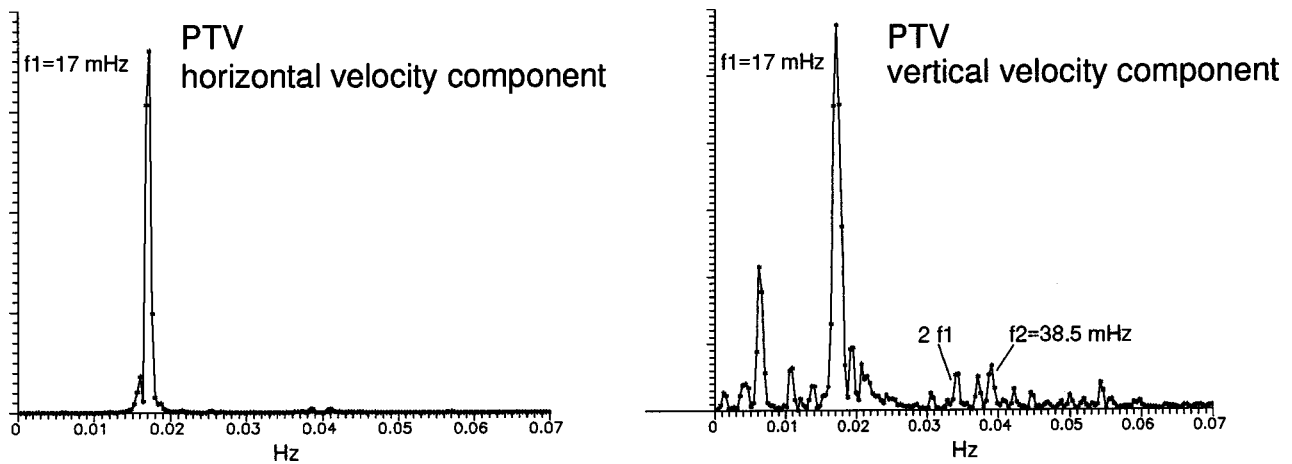

FIG. 15. PTV spectra of horizontal and vertical velocity components at the same point of LDA measurements: $Ra = 1.2 \times 10^7$. Water-glycerol 7.5% mixture.
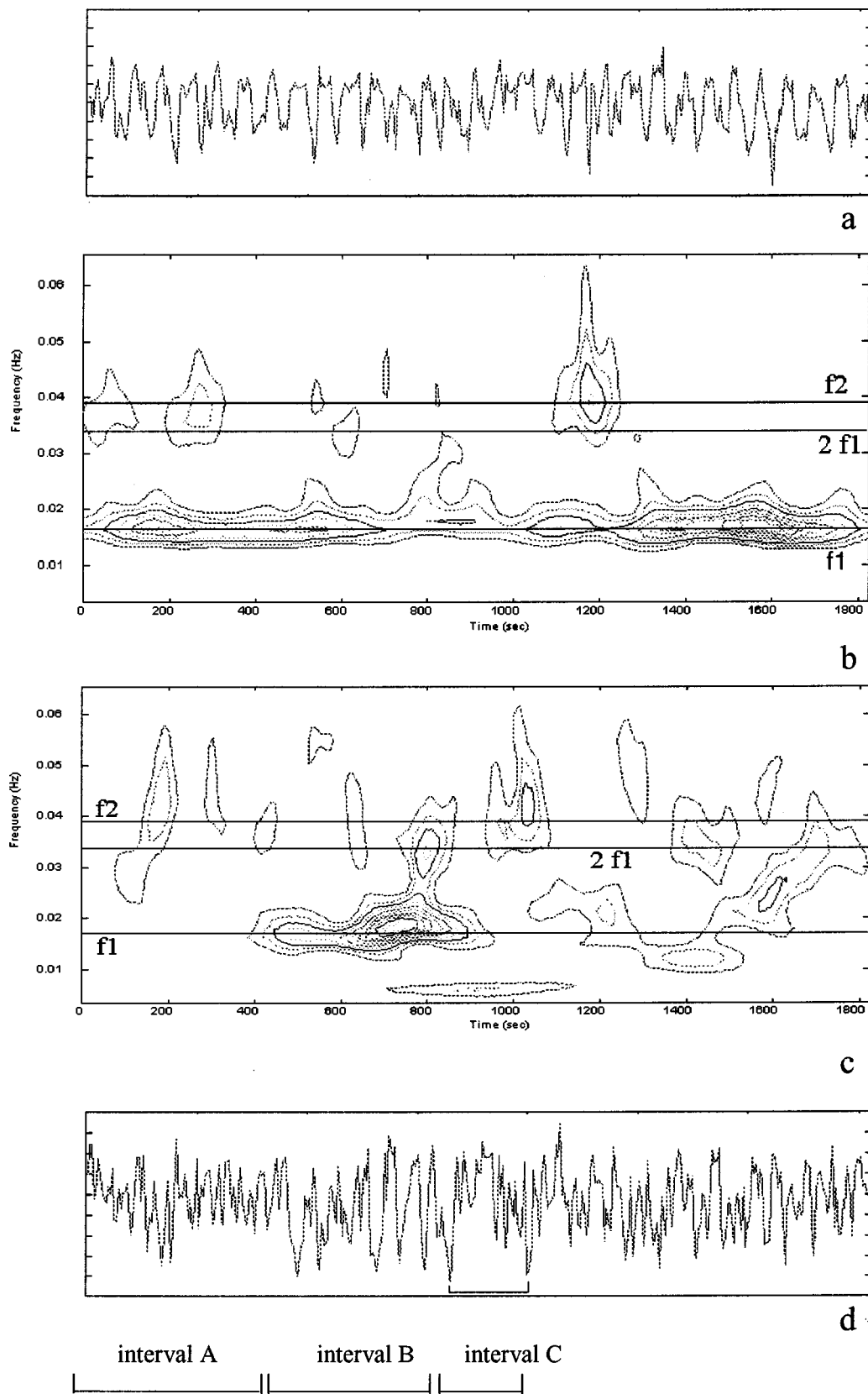
FIG. 16. Time histories of horizontal (a) and vertical (d) velocity components. Local WT spectrum of horizontal (b) and vertical (c) velocity components. Same point of LDA measurements: $Ra = 1.2 \times 10^7$, water-glycerol 7.5% mixture.

placed toward one side of the vessel, the expected frequencies are the same for the vertical and horizontal components. A careful examination of the time histories obtained from PTV measurements (Fig. 16), using the modulus of WT, shows that there are substantial variations in the instantaneous frequency content of the two velocity components. The horizontal component preserves the same fundamental frequency ($f_1 \sim 17$ mHz) throughout all the acquisition time,

showing a few contributions at the second frequency ($f_2 \sim 38$ mHz). On the other hand, the vertical component oscillates at the fundamental frequency for a definite time interval (400 s$<t<900$ s), while the second frequency appears occasionally. This velocity component seems to be much less stable than the horizontal: therefore, the vertical component is used to individuate time intervals in Fig. 16(d). Being the second frequency approximately double than the main one (as observed in LDA measurements), a strong coupling between the oscillation of the plume (related to $2f_1$) and the traveling of a blob (related to f_2) is suggested. In one time window [800 s$<t<1000$ s, labeled C in Fig. 16(d)] a small frequency at about $f=6$ mHz appears: it is connected to a strong local fluctuation between two minima on a time-scale of the order of 200 s, which is close to the inverse of the observed frequency f. This value is not a subharmonic of the main frequencies ($f_1/f \approx 2.8$, $f_2/f \approx 6.3$).

Two fundamental regimes can be summarized:
(i) for 0 s$<t<400$ s, the horizontal velocity oscillates at f_1 and the vertical mainly at f_2 and $2f_1$. The amplitude of positive and negative oscillations is almost equal. This time interval corresponds to oscillations of the plume perturbed by the presence of blobs symmetrically emitted toward the right and left hand side of the vessel (time interval A in Fig. 16).
(ii) for 400 s$<t<900$ s, the two components oscillate at almost the same frequency f_1. The vertical velocity component shows amplitude of negative oscillations larger than in time interval A. This corresponds to a maximum vertical component when the plume is inclined toward one side of the vessel, that is to a nonsymmetric configuration (time interval B in Fig. 16).

In the remains of the time interval the two regimes reproduce this behavior.

The physical picture may be described as follows. The linear heating channel originates a raising thermal plume leading to two counterrotating vortices. At small Rayleigh number this configuration is steady, whereas at higher values it starts to oscillate on the vertical plane. For a further increase, the previous regime is perturbed by the presence of isolated hot and cold fluid elements. Usually blobs move the plume symmetrically, but sometimes they force the plume toward one side of the vessel in a nonsymmetrical pattern.

It is important to connect this behavior to the spatial flow configuration. This is done by observing the PTV flow fields in time. In Fig. 17 the basic flow configurations for time intervals A and B are plotted. The time interval A (0 s$<t<400$ s) is characterized by an oscillation of the flow configuration toward the left and right side of the vessel [Figs. 17(a),(b)]. As previously noticed, the frequency of such an oscillation for the vertical component is almost double than for the horizontal. The amplitude of the oscillations is almost the same when the plume is directed toward the right or the left hand side of the vessel. The vertical velocity at the center is always positive. This is the main flow regime, and it is observed throughout the whole acquisition interval, giving the sharp peak at $f_1 \approx 17$ mHz. In the time interval B (400 s$<t<900$ s) the overlapping of the previous oscilla-
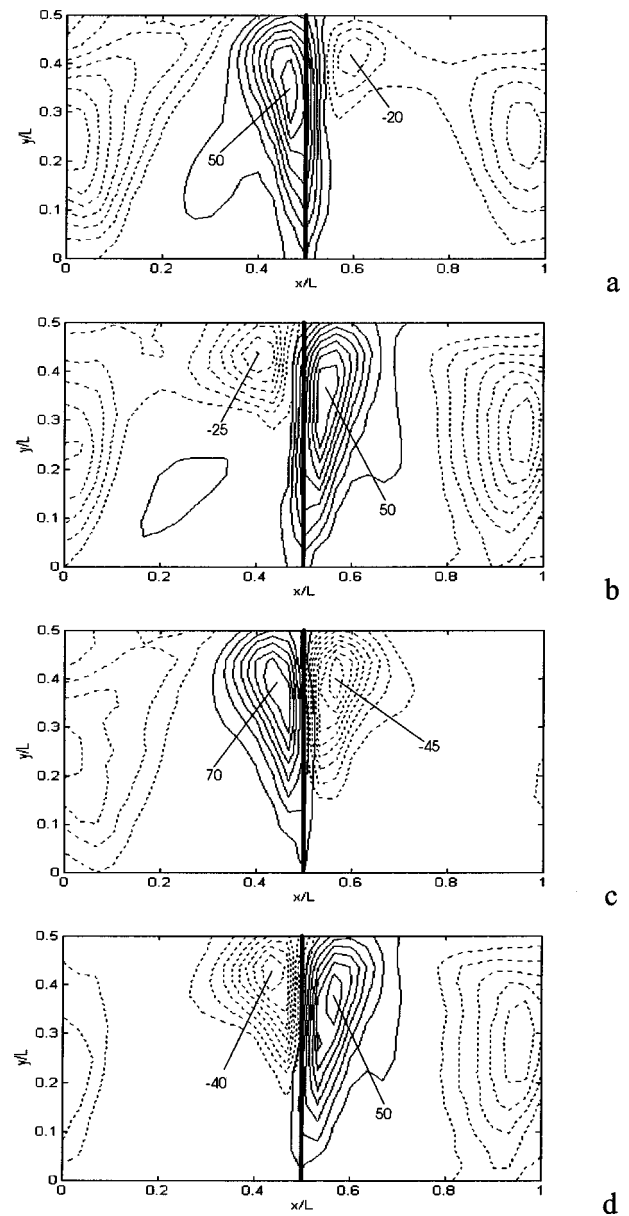

FIG. 17. Isocontours of the vertical velocity component: positive (continuous lines) and negative (dotted lines). Time interval A (a,b), time interval B (c,d). The maximum and minimum values (in arbitrary units) are given. The vertical thick lines indicate the symmetry axis. Same point of LDA measurements: Ra$=1.2\times10^7$, water-glycerol 7.5% mixture.

tion with a nonsymmetric flow configuration is observed. It causes the vertical velocity component to be negative on the upper part of the symmetry axis: The resulting flow field [Figs. 17(c),(d)] oscillates between a nearly symmetric configuration [Fig. 17(d)] and a nonsymmetric configuration characterized by large positive and negative vertical velocity values [Fig. 17(c)]. This large velocities correspond to those observed in Fig. 16 during the time interval B.

V. CONCLUDING REMARKS

The combined use of single-point (LDA) and multi-point (PTV) nonintrusive measurement techniques allows to investigate the behavior of an unstable convective flow: the connection between the time evolution and the spatial configu-

ration is achieved by these methods. This connection reflects a coupling between spatial and temporal modes that has been already observed in other convective flows (Rubio *et al.*[22]). The Wavelet Transform is employed to detect sharp changes in the velocity time histories. The following statements should be retained by the present analysis:

(i) The results are in fairly good agreement with experimental and numerical studies of similar systems. However, it should be noted that, due to the presence of the linear heating channel, the time evolution recorded at one point of the field exhibits sharp transitions between different regimes. This is observed even when the control parameters are kept constant. From the present measurements it is found that the basic mechanism for transition is related to type II intermittency, and this is one of the few experimental examples of such a transition in a fluid. However, at some Rayleigh numbers, type III intermittency cannot be completely ruled out.

(ii) LDA measurements at one point of the field reveal that the coupling between the main frequency and a second frequency (almost twice the main one) is responsible for the loss of stability of the system. PTV measurements depict that this is valid all over the field. These two frequencies are never observed together, but they alternate in different time windows. The transition from one state to the other has an intermittent character and this is confirmed by the Global WT spectrum and by the distribution of time durations of regular windows.

(iii) PTV measurements make it possible to connect the frequencies to the spatial configurations. The time intervals characterized by the main frequency in the horizontal component and the second one (almost twice the main one) in the vertical component are characterized by two counterrotating rolls oscillating symmetrically in the vertical plane. On the other hand, the system sometimes exhibits a nonsymmetrical regime in which the velocity components display different values between left and right hand oscillations (with vertical and horizontal velocity components oscillating at almost the same frequency).

In involving further comparisons, it should be noted that there is an effect due to the position of the heating channel over the bottom plate. As already mentioned, Desrayaud and Lauriat[10] obtained a second frequency at about 1/10 of the main one: the heating channel was located at 1/3 of the height of the vessel, H. This frequency has been never found in the present measurements, suggesting that the height of the heating channel is crucial to the process by which the system selects the way for the flow to become unstable. Preliminary numerical and experimental tests on the same vessel geometry, locating the heating channel at about $H/3$, confirm the presence of the frequency $f_1/10$, and show that stability is lost through the interaction of these two frequencies.

The overall conclusion of the paper is that the investigated convective flow is extremely sensitive to variations of the external parameters (i.e., of Rayleigh and Prandtl numbers), to the vessel geometry (length, width, and aspect ratio), and to the position of heating elements. Nevertheless, the investigation of the different effects leading to instabilities makes the control of such a fluid flow a possible challenge for fluid dynamicists.

[1] P. Welander, ''On the oscillatory instability of a differentially heated fluid loop,'' J. Fluid Mech. **29**, 17 (1967).

[2] E. L. Koschmieder, *Benard Cells and Taylor Vortices* (Cambridge University Press, Cambridge, 1993).

[3] R. Krishnamurti, ''On the transition to turbulent convection. Part 1. The transition from two- to three-dimensional flow,'' J. Fluid Mech. **42**, 295 (1970).

[4] R. Krishnamurti, ''On the transition to turbulent convection. Part 2. The transition to time dependent flow,'' J. Fluid Mech. **42**, 309 (1970).

[5] M. Lesieur, *Turbulence in Fluids* (Kluwer Academic, Dordrecht, 1990).

[6] A. C. Newell and J. A. Whitehead, ''Finite bandwidth, finite amplitude convection,'' J. Fluid Mech. **38**, (1969).

[7] F. H. Busse and J. A. Whitehead, ''Oscillatory and collective instabilities in large Prandtl number convection,'' J. Fluid Mech. **66**, 67 (1974).

[8] E. W. Bolton, F. H. Busse, and R. M. Clever, ''Oscillatory instabilities of convection rolls at intermediate Prandtl numbers,'' J. Fluid Mech. **164**, 469 (1986).

[9] R. M. Clever and F. H. Busse, ''Steady and oscillatory bimodal convection,'' J. Fluid Mech. **271**, 103 (1994).

[10] G. Desrayaud and G. Lauriat, ''Unsteady confined buoyant plumes,'' J. Fluid Mech. **252**, 617 (1993).

[11] E. Moses, G. Zocchi, and A. Libchaber, ''An experimental study of laminar plumes,'' J. Fluid Mech. **251**, 581 (1993).

[12] A. Schluter, D. Lortz, and F. H. Busse, ''On the stability of steady finite amplitude convection,'' J. Fluid Mech. **23**, 129 (1965).

[13] J. P. Gollub and S. V. Benson, ''Many routes to turbulent convection,'' J. Fluid Mech. **100**, 449 (1980).

[14] F. H. Busse, ''The oscillatory instability of convection rolls in a low Prandtl number fluid,'' J. Fluid Mech. **52**, 97 (1972).

[15] R. J. Adrian and C. S. Yao, ''Power spectra of fluid velocities measured by laser Doppler velocimetry,'' Exp. Fluids **5**, 17 (1987).

[16] M. Benak, M. Sturm, and C. D. Tropea, ''Correlation estimators for two-point laser Doppler anemometry,'' in *Laser Anemometry-Advances and Applications*, SPIE **2052**, 613 (1993).

[17] J. C. Agui and J. Jimenez, ''On the performance of particle tracking,'' J. Fluid Mech. **185**, 447 (1987).

[18] G. R. Spedding and E. J. M. Rignot, ''Performance analysis and application of grid interpolation techniques for fluid flows,'' Exp. Fluids **15**, 417 (1993).

[19] M. Farge, ''Wavelet transforms and their applications to turbulence,'' Annu. Rev. Fluid Mech. **24**, 395 (1992).

[20] P. Bergé, Y. Pomeau, and C. Vidal, *Order Within Chaos* (Wiley-Interscience, New York, 1984).

[21] P. Manneville and Y. Pomeau, ''Different ways to turbulence in dissipative dynamical systems,'' Physica D **1**, 219 (1980).

[22] M. A. Rubio, P. Bigazzi, L. Albavetti, and S. Ciliberto, ''Spatio-temporal regimes in Rayleigh–Benard convection in a small rectangular cell,'' J. Fluid Mech. **209**, 309 (1989).